NASA TECHNICAL NOTE




NASA TN D-8354

# DIRECTIONALLY SOLIDIFIED IRON-BASE EUTECTIC ALLOYS

*Surendra N. Tewari*

*Lewis Research Center*
*Cleveland, Ohio 44135*

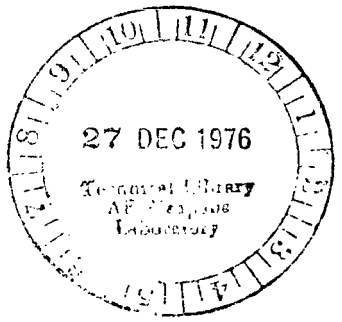



NATIONAL AERONAUTICS AND SPACE ADMINISTRATION • WASHINGTON, D. C. • DECEMBER 1976

| 1. Report No. | 2. Government Accession No. | 3. Recipient's Catalog No. |
|---|---|---|
| NASA TN D-8354 | | |

| 4. Title and Subtitle | 5. Report Date |
|---|---|
| DIRECTIONALLY SOLIDIFIED IRON-BASE EUTECTIC ALLOYS | December 1976 |
| | 6. Performing Organization Code |

| 7. Author(s) | 8. Performing Organization Report No. |
|---|---|
| Surendra N. Tewari | E-8846 |
| | 10. Work Unit No. |
| | 505-01 |

| 9. Performing Organization Name and Address | 11. Contract or Grant No. |
|---|---|
| Lewis Research Center<br>National Aeronautics and Space Administration<br>Cleveland, Ohio 44135 | |
| | 13. Type of Report and Period Covered |
| 12. Sponsoring Agency Name and Address | Technical Note |
| National Aeronautics and Space Administration<br>Washington, D.C. 20546 | 14. Sponsoring Agency Code |

15. Supplementary Notes

16. Abstract

Pseudobinary eutectic alloys with nominal compositions of Fe-25Ta-22Ni-10Cr and Fe-15.5Nb-14.5Ni-6.0Cr were directionally solidified at 0.5 centimeter per hour. Their microstructure consisted of the fcc, iron solid-solution, matrix phase reinforced by about 41-volume-percent, hcp, faceted $Fe_2Ta$ fibers and 41-volume-percent, hcp, $Fe_2Nb$ lamellae for the tantalum- and niobium-containing alloys, respectively. The microstructural stability under thermal cycling and the temperature dependence of tensile properties were investigated. These alloys showed low elevated-temperature strength and are not considered suitable for application in aircraft-gas-turbine blades although they may have applicability as vane materials.

17. Key Words (Suggested by Author(s))

Iron alloys; Heat-resistant alloys; Turbine blades; Mechanical properties; Eutectic alloys; Cast alloys; Microstructure; Ductility; Oxidation resistance

18. Distribution Statement

Unclassified - unlimited

STAR Category 26

| 19. Security Classif. (of this report) | 20. Security Classif. (of this page) | 21. No. of Pages | 22. Price* |
|---|---|---|---|
| Unclassified | Unclassified | 24 | $3.50 |

* For sale by the National Technical Information Service, Springfield, Virginia 22161

# DIRECTIONALLY SOLIDIFIED IRON-BASE EUTECTIC ALLOYS*

by Surendra N. Tewari

Lewis Research Center

SUMMARY

In the research reported herein the $\gamma$-$\epsilon$ pseudobinary eutectic compositions in the Fe-Ta-Ni-Cr and Fe-Nb-Cr systems were identified and directionally solidified, and their suitability as an advanced aircraft-gas-turbine blade material was investigated.

The nominal eutectic alloy compositions (in wt %) of Fe-15.5Nb-14.5Ni-6.0Cr and Fe-25Ta-22Ni-10Cr had freezing ranges from 1344° to 1313° C and from 1364° to 1332° C, respectively. Their directional solidification at 0.5 centimeter per hour in a modified Bridgman furnace with a melt temperature of about 1760° C resulted in the formation of niobium (or tantalum) oxide and aluminum oxide inclusions. A melt temperature of about 1680° C yielded a relatively inclusion-free length of 6 centimeters at the bottom of the bar, which was used for tensile property measurements.

The alloys were directionally solidified at 0.5 centimeter per hour with a temperature gradient of about 200° C per centimeter at the liquid-solid interface. The microstructure of the tantalum-containing alloy consisted of about 41-volume-percent, faceted, $Fe_2Ta$ fibers imbedded in an iron, solid-solution matrix. The microstructure of the niobium-containing alloy consisted of alternating lamellae of about 41-volume-percent $Fe_2Nb$ phase and the iron, solid-solution phase.

The tantalum-containing alloy did not show any microstructural degradation following 1800 thermal cycles from 1100° to 425° C (3-min interval) in an oxidation-erosion burner apparatus. The niobium-containing alloy was not investigated for its microstructural stability under thermal cycling.

The tensile strengths of the alloys decreased from about 800 to 900 MPa at room temperature to about 175 MPa at 1100° C. The reduction in area increased from less than 2 percent at room temperature to about 3 to 9 percent at 1100° C.

Based on this investigation the Fe-25Ta-22Ni-10Cr and Fe-15.5Nb-14.5Ni-6.0Cr eutectics are not suitable for aircraft-gas-turbine blade materials because of their low elevated-temperature strength and their solidification processing problems. However, they may have application as vane materials by further composition modification.

---

*Presented in part at the 105th Annual Meeting of the American Institute of Mining, Metallurgical, and Petroleum Engineers, Las Vegas, Nevada, February 22-26, 1976.

†National Research Council - National Aeronautics and Space Administration Research Associate.

## INTRODUCTION

Directionally solidified eutectic alloys are presently being considered as the next generation of aircraft-gas-turbine blade materials. Their use is expected to result in significant engine performance advantages because of their $50^{\circ}$ to $100^{\circ}$ C increase in allowable metal temperatures over superalloys (ref. 1). The eutectic alloys being investigated for such an application generally have a nickel- or cobalt-base matrix that is reinforced by intermetallic fibers or lamellae (ref. 2). A lamellar, $Ni_3Nb$-reinforced, nickel-base alloy ($\gamma/\gamma' - \delta$, ref. 3) and a fibrous, TaC-reinforced, cobalt-base alloy (CoTaC, ref. 4) have probably received the most intensive investigation. Identification and development of new, potentially promising eutectic systems with properties superior to $\gamma/\gamma' - \delta$ or CoTaC are desirable.

Since the mechanical properties of the reinforcing intermetallic phases are generally not known, it is not possible to select a potentially promising eutectic system based on this criterion. Therefore, one must consider such properties as the eutectic melting point, the density of the phases, the volume fraction of the reinforcing phase, the possibility of solid-solution and precipitation strengthening of the phases, the possibility of alloying for improved oxidation resistance, the absence of any allotropic transformations, and a relatively constant mutual solubility of the phases as a function of temperature. The last two characteristics are needed to provide microstructural stability under thermal cycling.

The Fe-Ta-Ni-Cr and Fe-Nb-Ni-Cr systems were selected for this study because they appeared attractive based on the foregoing property criteria. Depending on the Fe/Ni ratio the matrix was expected to be a body-centered cubic (bcc) or face-centered cubic (fcc) solid-solution phase, and the reinforcing phase was expected to be hexagonal $Fe_2Ta$ or $Fe_2Nb$. A directionally solidified, Fe-23Cr-13.3Nb, pseudobinary eutectic alloy had been prepared and previously examined by Jaffrey and Marich (ref. 5). However, they could not achieve plane front solidification and therefore produced an alloy with a cellular microstructure.

Temperature-dependent allotropic transformations have been shown to be a potential source of microstructural instability under thermal cycling (ref. 6). The Fe-Nb and Fe-Ta binary eutectic compositions reported in reference 7 were modified by nickel additions to stabilize the fcc, iron solid-solution phase. Chromium additions were further made to the alloys to improve their oxidation resistance.

In this investigation iron-base eutectic alloys reinforced by the $\epsilon$-phase ($Fe_2Ta$ or $Fe_2Nb$) were directionally solidified and studied to determine their suitability as aircraft-gas-turbine blade materials. Their microstructural stability under thermal cycling and the temperature dependence of their tensile properties were studied.

## MATERIALS, APPARATUS, AND PROCEDURE

### Materials

The purities of raw materials used in this study are shown in table I.

### Apparatus

The directional solidification apparatus, which is a modified Bridgman furnace, is shown in figure 1. The crucible containing the ingot was heated by radiation from a graphite susceptor positioned inside an induction coil. The alumina heat shield surrounding the graphite susceptor was used to minimize the heat loss from the susceptor. The power was supplied by a 7.5-kilowatt radiofrequency generator operating at 400 kilohertz. For any given power setting a flat liquid-solid interface was obtained just below the induction coil by adjusting the thickness of the alumina spacer between the susceptor and the water-spray chill ring. The induction coil was more densely wound at the bottom to provide greater localized heating at the solid-liquid interface.

### Procedure

Master melting. - Initial 1.2-kilogram heats were melted in a 50-kilowatt, 10-kilohertz induction furnace in calcia-stabilized zirconia crucibles. The environment was first evacuated and then partially backfilled with argon. The melts were poured into preheated zircon shell molds to make cylindrical bar ingots (1-cm diam, 16-cm length) for subsequent directional solidification. Each shell mold provided six bar ingots.

Bleedout and eutectic composition determination. - The approximate eutectic composition was obtained by the eutectic bleedout technique (ref. 8). A bar ingot of the off-eutectic composition alloy was slowly heated in the Bridgman furnace. Eutectic regions on the bar surface, being the lowest melting-point constituent, melted first and solidified in a sleeve-like appearance at the bottom of the bar. This eutectic bleedout material was analyzed by spectrochemical analysis, and thus the first approximation of the eutectic alloy composition was obtained. The bleedout technique was repeated on the first approximation alloy, thus yielding the base-alloy compositions used for subsequent directional solidification and property evaluations. Freezing ranges of the base-alloy compositions were determined by a differential thermal analysis technique.

Directional solidification. - The bar ingots obtained from the master melting were remelted and directionally solidified in an alumina tube crucible (1.3-cm i.d., 1.8-cm o.d., 30-cm length) in a modified Bridgman furnace (fig. 1) under a flowing argon

atmosphere. Directional solidification was obtained by lowering the crucible through a water-spray chill ring at a constant speed of 0.5 centimeter per hour. The temperature gradient in the liquid at the liquid-solid interface was determined to be about 200° C per centimeter. The melts were maintained at a superheat of about 300° C. Typical directionally solidified bar lengths were 10 centimeters. A total of 12 bars were directionally solidified. Each bar yielded one specimen for mechanical testing.

Inspection and mechanical testing. - A flat was ground on the bar surface along its length, polished and etched electrolytically at room temperature in a solution of 0.45 liter of water, 0.015 liter of hydrofluoric acid, 0.005 liter of nitric acid, and 0.010 liter of sulfuric acid to observe the degree of alinement along the length of the bar. Directionally solidified bars with well-alined microstructures were ground to the specimen dimension shown in figure 2. Machined specimens were inspected by X-ray radiography and fluorescent dye penetrant to detect any internal or surface voids or cracks. Tensile tests were conducted at 25°, 750°, and 1100° C in air at a constant crosshead speed of 1.2 centimeters per minute. All tests were loaded parallel to the alloy growth direction.

Thermal cycling. - The 1.2-centimeter-diameter directionally solidified bar was subjected to 1800 thermal cycles in a burner apparatus similar to the one used by Johnston and Ashbrook (ref. 9). The alloy was heated quickly to 1100° C in the blast of a combustion gas stream (Mach 0.3) achieved by burning a mixture of JP-5 jet fuel and air. The alloy was held in the jet for 2 minutes and then quickly cooled to 425° C in a blast of room-temperature air at Mach 0.7. The elapsed time for each cycle was 3 minutes. The bar was taken out at regular intervals and weighed to record the weight loss as a function of the number of cycles.

Metallography. - The microstructure and the eutectic phase alinement of the alloys were examined by light metallography. Specimens were mounted in Bakelite and polished by normal metallographic procedures, with a final polish of 0.5-micrometer alumina on microcloth. Specimens were electrolytically etched in the same etchant that was used for the inspection. Scanning electron microscopy (SEM) was used for fracture examination.

## RESULTS AND DISCUSSION

### Directional Solidification

The nominal eutectic alloy compositions identified by the eutectic bleedout technique (ref. 8) and selected for directional solidification were Fe-25Ta-22Ni-10Cr and Fe-15.5Nb-14.5Ni-6.0Cr (in wt %). The tantalum- and niobium-containing alloys had freezing ranges from 1364° to 1332° C and from 1344° to 1313° C (figs. 3(a) and (b), respectively).

Under the liquid-solid-interface temperature gradient of 200° C per centimeter and a maximum melt temperature of about 1760° C (about 400° C superheat), alined microstructures were obtained for a growth speed of 0.5 centimeter per hour. This relatively slow growth speed resulted in melt-mold contact times as long as 20 hours. The presence of trapped inclusions in the alined microstructure was attributed to the resulting mold-metal reaction. The distribution and appearance of these inclusions in the niobium-containing alloy are shown in figure 4. Similar inclusions were observed in the tantalum-containing alloy that was solidified under the same conditions. The micrographs that are from transverse (perpendicular to the alloy growth direction) sections at 2.6 and 8.5 centimeters from the bottom end of the bar clearly show the increase in the size and number of the inclusions as the solidification progressed. These inclusions also are believed to have contributed to formation of the hot-tear microcracks observed in the microstructure (fig. 4(b) and its inset). The morphology of the inclusions is shown in more detail at higher magnification in the inset of figure 4(a). There are actually two kinds of inclusions intertwined: one light in shade, the other darker. As solidification progressed (from bottom to top of the bar) the lighter (wider) inclusions diminished in size and number, and only the darker ones (cruciform-shaped inside) were observed in the last portion to solidify.

These inclusions were identified by electron microprobe X-ray analysis as shown in the secondary electron and X-ray micrographs of figure 5. The aluminum $K_\alpha$ X-ray micrograph of figure 5(b) shows the narrow, cruciform inclusion to be aluminum rich. The wider type of inclusion appears to be niobium rich in a niobium $L_\alpha$ X-ray micrograph (fig. 5(c)). Both inclusions were observed to be oxygen rich (fig. 5(d)). The possibility that the image contrast in figure 5(d) may have been caused by differences in X-ray background and may not be related to the presence of oxygen was investigated by observing the oxygen X-ray spectral peak with a beam on one of the inclusions. A peak in the oxygen X-ray spectrum showed that these inclusions were indeed oxygen rich. The two inclusions were therefore identified as aluminum and niobium oxides.

The mold-metal reaction responsible for these inclusions can be decreased either by using a different crucible, by changing the alloy chemistry (a smaller freezing range alloy could be alined at a higher growth rate), or by decreasing the maximum superheat in the melt. An attempt was made to replace the recrystallized alumina crucible with an alumina-stabilized zirconia crucible. However, the zirconia crucible could not withstand the thermal shock from the water-spray quench and cracked. The melt superheat was decreased by about 80° C, thereby decreasing the maximum melt temperature to about 1680° C and resulting in about 90 percent less oxide inclusions. The alloys could not be alined at growth speeds higher than 0.5 centimeter per hour. The bottom 6 centimeters of the bar, which was relatively free of the inclusions (at 6 cm from the bottom the oxide particles were of the size and distribution shown in fig. 4(a)), was used to investigate the mechanical properties of the directionally solidified eutectic alloys.

Chromium is known to increase the alloy freezing range in several alloys, for example, $\gamma/\gamma' - \delta$ (ref. 10). In this reference, critical G/R values (where G is the temperature gradient in a liquid at the liquid-solid interface and R is the growth speed) required for a plane front solidification of $\gamma/\gamma' - \delta$ eutectic alloys were observed to increase with increasing chromium concentration (ref. 10). Therefore, the possibility that, by reducing the chromium content, the alloy freezing range could be decreased and the alloy could be alined at higher growth speeds was also investigated. This would decrease the mold-melt contact time. Two more eutectic alloys with decreasing chromium content, Fe-16.0Nb-14.9Ni-3.0Cr and Fe-16.5Nb-15.4Ni (nominal wt %), were directionally solidified under the same solidification conditions used for the other alloys tested (maximum melt temperature of $1680^{\circ}$ C). These two alloys, however, still could not be alined at growth speeds higher than about 0.5 centimeter per hour. This observation suggests that, in this alloy system, chromium does not have a large influence on the freezing range.

## Growth Morphology

Niobium-containing eutectic alloy. - Figure 6 shows the longitudinal (parallel to the alloy growth direction) and transverse microstructures of the directionally solidified niobium-containing eutectic alloy (Fe-15.5Nb-14.5Ni-6.0Cr). The microstructure can be seen to consist of alternating lamellae of fcc, iron solid-solution ($\gamma$) and hcp, intermetallic $Fe_2Nb$ ($\epsilon$) phases. The approximate compositions of the phases (in wt %) as determined by the electron microprobe analysis are Fe-33.7Nb-9.8Ni-4.5Cr for the intermetallic lamellae and Fe-1.5Nb-15.6Ni-7.5Cr for the matrix phase (average of 10 analyses of each phase). X-ray diffraction analysis of the directionally solidified eutectic alloy showed the lattice parameters to be 3.55 angstroms for the fcc matrix and 4.82 and 7.87 angstroms for the c- and a-directions, respectively, of the hcp phase. The volume fraction of the intermetallic phase determined according to a new ASTM recommended practice (ref. 11) is $0.41 \pm 0.02$.

Fault boundaries formed by two adjacent regions of lamellae with slight misalinement can be seen in the transverse microstructure (fig. 6(b)). Unlike Jaffrey and Marich (ref. 5), who observed both the fibrous (at the cell center) and the lamellar (at the cell boundaries) microstructures, only the lamellar microstructure was observed in this investigation. Jaffrey and Marich were not able to obtain a plane front solidification of their Fe-23Cr-13.3Nb eutectic alloy and as a result observed only cellular microstructures. Probably the lamellar morphology is the more energetically favored one for the Fe-15.5Nb-14.5Ni-6.0Cr composition, and as a result only lamellar microstructure was obtained in the present work under plane front solidification conditions.

Tantalum-containing eutectic alloy. - Figure 7 shows the longitudinal and transverse microstructures of the directionally solidified Fe-25Ta-22Ni-10Cr eutectic alloy. The microstructure consists of hcp, intermetallic $Fe_2Ta$ ($\epsilon$) fibers imbedded in an fcc, Fe-Ni solid-solution ($\gamma$) matrix. The approximate compositions (in wt %) as determined by the electron microprobe X-ray analysis are Fe-45.0Ta-14.1Ni-7.0Cr for the intermetallic phase and Fe-4.4Ta-29.5Ni-12.3Cr for the matrix phase (average of 10 analyses of each phase). These fibers appear to be faceted when viewed at higher magnifications. Some fibers can be seen joining and forming plates in the transverse section (fig. 7(b)) in a manner similar to that observed in an Al-$Al_3Ni$ eutectic alloy (ref. 12). Less than 10 percent of the cross-sectional area contained such plates.

Note that the microstructure is fibrous despite the large volume fraction, 0.41±0.03, of the second phase. It is believed that the volume fraction of the second phase (which according to ref. 13 should be fibrous in the absence of any surface-energy anisotropy only up to 0.28 volume fraction), the growth velocity of the alloy (ref. 14), and the surface-energy anisotropy of the interface (ref. 13) are the factors that determine whether the directionally solidified eutectic microstructure will be fibrous or lamellar. However, the exact reasons why similar phases ($Fe_2Nb$ against $Fe_2Ta$) should develop different microstructures in a similar matrix under the same solidification conditions are not understood.

## Thermal Cycling

Directionally solidified, lamellar eutectic alloys are generally known to possess good microstructural stability during thermal cycling (refs. 15 and 16). Fibrous eutectic alloys, on the other hand, frequently have shown microstructural instability during thermal cycling (ref. 17). The Fe-25Ta-22Ni-10Cr fibrous eutectic alloy was therefore subjected to thermal cycling in air between 1100° and 425° C, in 3-minute cycles, to investigate its microstructural stability under thermal cycling. After 1800 cycles the microstructure of the alloy was examined. Significant microstructural instability of $Fe_2Ta$ fibers due to thermal cycling was not observed (fig. 8). There was only occasional evidence of fiber pinchoff following the thermal cycling (fig. 8(b)). It is believed that if this alloy were subjected to a substantially larger number of cycles, the $Fe_2Ta$ fibers would break down into segments. These could eventually coarsen and spheroidize, as was observed for chromium fibers in a directionally solidified NiAl-Cr eutectic alloy (ref. 18). The surface oxidation of the alloy was observed to a depth of about 150 micrometers. Below an oxide scale of about 150 micrometers a region of about 60 micrometers can be seen where only preferred oxidation of the $Fe_2Ta$ phase has taken place (fig. 8(c)). Since tantalum is more susceptible to oxidation than the nickel-base solid solution, preferred oxidation of the $Fe_2Ta$ phase is to be expected.

No systematic study was made of the oxidation resistance of the alloy. However, measurements were made of the weight loss that occurred during thermal cycling, and the results are shown in figure 9. The Fe-25Ta-22Ni-10Cr eutectic alloy examined has slightly better oxidation resistance than the $\gamma/\gamma' - \delta$ eutectic alloy (ref. 15). However, its oxidation resistance is much inferior to that of B-1900, which was subjected to approximately similar thermal cycling treatments.

Since preliminary measurements had shown that the Fe-15.5Nb-14.5Ni-6.0Cr eutectic alloy had low elevated-temperature strength, its microstructural stability under thermal cycling was not investigated. However, this alloy is lamellar and is therefore expected to show good microstructural stability under thermal cycling. Its oxidation resistance is probably poor, similar to that of the Fe-25Ta-22Ni-10Cr alloy discussed previously because niobium is similar to tantalum in its chemical affinity for oxygen.

## Mechanical Properties

Tantalum-containing eutectic alloy. - The temperature dependence of the tensile properties of the Fe-25Ta-22Ni-10Cr eutectic alloy is shown in table II and figure 10. The ultimate tensile strength of the alloy decreased with increasing temperature from about 900 MPa at room temperature to about 175 MPa at $1100^{\circ}$ C. Also note in this figure that the elevated-temperature strength properties of this alloy are much inferior to those of the $\gamma/\gamma' - \delta$ alloys currently under investigation (ref. 3). The strength values appear still less attractive when one compares the density of 9.1 $g/cm^2$ (measured for this alloy) with 8.6 $g/cm^3$ for $\gamma/\gamma' - \delta$. The Fe-25Ta-22Ni-10Cr eutectic alloy therefore does not have sufficient strength to compete with $\gamma/\gamma' - \delta$ alloys for gas-turbine blade applications.

The Fe-25Ta-22Ni-10Cr alloy exhibited low ductility (fig. 10). The reduction-in-area values, however, cannot be considered representative of the alloy capability since oxide particles were abundant. The presence of these oxide particles in the fracture region is expected to adversely affect the alloy ductility (ref. 19). Based on the fracture examination discussed in the next paragraph, the alloy without any oxide inclusions would be expected to possess low ductility at room temperature and $750^{\circ}$ C; however, at $1100^{\circ}$ C it should show considerably more ductility than the observed 3 to 8 percent reduction in area indicates (fig. 10).

The microstructural features of tensile fracture in the Fe-25Ta-22Ni-10Cr alloy are shown in figure 11. A longitudinal section through the room-temperature tensile fracture (fig. 11(a)) shows the brittle $Fe_2Ta$ fiber fracture between ductile regions of the matrix. Occasional cracking of fibers immediately below the fracture surface and some evidence of fiber pullout can also be observed in this figure. Figure 11(b), a SEM micrograph of the room-temperature fracture surface, shows more clearly the ductile

necked failure of the matrix and the brittle failure of fibers with shattered ends. A longitudinal section through a 750° C tensile fracture (not shown) also showed similar brittle fiber failure and ductile failure of the matrix. The corresponding elevated-temperature, 1100° C, fracture (fig. 11(c)) on the other hand showed that the fibers had broken into short segments close to the fracture surface. The surrounding matrix, however, filled up the cracks created by such fiber segmentation and very few voids were observed. This type of fiber segmentation is expected to result in higher ductility at 1100° C (fig. 10) in the absence of oxide inclusions. The oxide film at the fracture surface (fig. 11(c)) was observed because the tests were conducted in air.

Niobium-containing eutectic alloy. - Figure 12 shows the temperature dependence of the tensile properties of the Fe-15.5Nb-14.5Ni-6.0Cr eutectic alloy. The alloy has an ultimate tensile strength of about 780 MPa at room temperature. The strength decreases with increasing temperature, and at 1100° C it is only 175 MPa. The alloy is also considerably weaker than the $\gamma/\gamma' - \delta$ eutectic alloy at elevated temperatures and is not considered suitable as an aircraft-gas-turbine blade material. It may also be noted in figure 12 that this alloy shows considerably more strength above 550° C than was observed for a directionally solidified, Fe-23Cr-13.3Nb eutectic alloy by Jaffrey and Marich (ref. 5). This strength increase over the alloys investigated in reference 5 may be due to a much better alined microstructure than the cellular microstructure of the reference 5 alloys, a higher volume fraction of $Fe_2Cb$ phase (41 percent against their 22 percent), and a fcc matrix phase against their bcc matrix.

The Fe-15.5Nb-14.5Ni-6.0Cr alloy has low ductility (fig. 12). The reduction in area is about 2 percent at room temperature and 750° C, although at 1100° C it is about 9 percent. However, as for the tantalum-containing alloy, if this alloy could be directionally solidified without any oxide inclusions, it would be expected to show improved ductility (especially at 1100° C, as evidenced by fracture morphology).

The microstructural features of tensile fracture in the Fe-15.5Nb-14.5Ni-6.0Cr eutectic alloy are shown in figure 13. The fracture behavior of the niobium-containing alloy is similar to that of the tantalum-containing alloy, except for the fact that the niobium-containing alloy is lamellar and the tantalum-containing alloy is fibrous. A longitudinal section through the room-temperature fracture surface (fig. 13(a)) shows the brittle fracture of the $Fe_2Nb$ lamellae and the ductile fracture of the matrix. Some evidence of broken sections of lamellae being pulled out at the fracture surface was also observed. The ductile, necked, failure mode of the matrix lamellae and the brittle, flat, $Fe_2Nb$ fracture are shown in figure 13(b), an SEM micrograph of the room-temperature fracture surface. A longitudinal section that passed through the 750° C tensile fracture surface (not shown) exhibited a fracture appearance very similar to the one at room temperature (i.e., ductile matrix and brittle $Fe_2Nb$ phase). Some ductility in the $Fe_2Nb$ fibrous phase above 700° C was observed by Jaffrey and Marich (ref. 5). No such ductility was observed here in $Fe_2Nb$ lamellae that failed due to 750° C tensile

fracture. The 1100° C tensile failure (fig. 13(c)) showed some ductility in both the matrix and the reinforcing phase. The $Fe_2Nb$ lamellae separated into segments and partially spheroidized in the region immediately below the fracture, causing occasional voids to form. Since these tests were conducted in air the fracture surfaces were heavily oxidized (fig. 13(c)).

## CONCLUDING REMARKS

In conclusion, the directionally solidified, iron-base eutectic alloys Fe-25Ta-22Ni-10Cr and Fe-15.5Nb-14.5Ni-6.0Cr have low elevated-temperature strength, low ductility at low to intermediate temperatures, and solidification processing problems (very low growth speed and resultant oxide inclusions). They are not considered suitable for application as aircraft-gas-turbine blade materials. However, they may have potential as vane materials, which are subjected to much lower stresses, particularly if oxide inclusions can be eliminated.

## SUMMARY OF RESULTS

Pseudobinary eutectic alloys with the nominal compositions (in wt %) of Fe-25Ta-22Ni-10Cr and Fe-15.5Nb-14.5Ni-6.0Cr were directionally solidified at 0.5 centimeter per hour in a modified Bridgman furnace having a temperature gradient of about 200° C per centimeter at the liquid-solid interface. Their microstructural stability under thermal cycling and the temperature dependence of their tensile properties were investigated. The following results were obtained from this study:

1. The Fe-25Ta-22Ni-10Cr and Fe-15.5Nb-14.5Ni-6.0Cr pseudobinary eutectic alloys had freezing ranges from 1364° to 1332° C and from 1344° to 1313° C, respectively.

2. Directional solidification at 0.5 centimeter per hour with a maximum melt temperature of about 1760° C resulted in the formation of trapped inclusions in the alined microstructure. These were identified as niobium (tantalum) oxide and aluminum oxide. A decreased melt temperature of about 1680° C resulted in a relatively inclusion-free bottom 6 centimeters of the directionally solidified bar, which was used for tensile property evaluation.

3. The microstructure of Fe-25Ta-22Ni-10Cr eutectic alloy consisted of about 41-volume-percent, hexagonal close packed (hcp), faceted $Fe_2Ta$ fibers imbedded in a face-centered-cubic (fcc), iron solid-solution matrix. The microstructure of the Fe-15.5Nb-14.5Ni-6.0Cr eutectic alloy consisted of alternating lamellae of about 41-volume-percent, hcp, $Fe_2Cb$ phase and the fcc, iron solid-solution phase.

4. The Fe-25Ta-22Nb-10Cr alloy did not show any microstructural degradation following 1800 thermal cycles. The niobium-containing alloy was not investigated for its microstructural stability under thermal cycling.

5. The Fe-25Ta-22Ni-10Cr alloy had a density of about 9.1 $g/cm^3$, and its tensile strength decreased from about 900 MPa at room temperature to about 175 MPa at 1100° C.

6. The Fe-15.5Nb-14.5Ni-6.0Cr alloy had a density of about 7.7 $g/cm^3$, and its tensile strength decreased from about 780 MPa at room temperature to about 175 MPa at 1100° C.

Lewis Research Center,
National Aeronautics and Space Administration,
Cleveland, Ohio, July 29, 1976,
505-01.

## REFERENCES

1. Jahnke, L. P.; and Bruch, C. A.: Requirements for and Characteristics Demanded of High Temperature Gas Turbine Components. Specialists Meeting on Directionally Solidified In Situ Composites. AGARD-CP-156, Advisory Group for Aerospace Res. and Develop., 1974, pp. 3-12.

2. Ashbrook, Richard L.: Directionally Solidified Composite Systems under Evaluation. Specialists Meeting on Directionally Solidified In Situ Composites. AGARD-CP-156, Advisory Group for Aerospace Res. and Develop., 1974, pp. 93-115.

3. Lemkey, F. D.; and McCarthy, G.: Quaternary and Quinary Modifications of Eutectic Superalloys Strengthened by $\delta$, $Ni_3Cb$ Lamellae and $\gamma'$, $Ni_3Al$ Precipitates. (R911698-13, United Aircraft Corp.; NAS3-17785) NASA CR-134678, 1975.

4. Bibring, H.: Mechanical Behavior of Unidirectionally Solidified Composites. Proceedings of Conference on In Situ Composites, vol. 2, Nat. Res. Council, 1972, pp. 1-69.

5. Jaffrey, D.; and Marich, S.: An Fe-Cr-Nb Pseudobinary Eutectic Alloy, Met. Trans., vol. 3, no. 2, Feb. 1972, pp. 551-558.

6. Arnson, H. L.: The Effect of Thermal Cycling on the Structure of the Co-$Co_3Cb$ Eutectic. AFML-TR-72-286, Air Force Mat. Lab. (AD-763706), 1972.

7. Metals Handbook. Vol. 8, 8th ed., Am. Soc. for Metals, 1973.

8. Kim, Y. G.; and Ashbrook, R. L.: Directionally Solidified Pseudobinary Eutectics of Ni-Cr-(Hf, Zr). NASA TM X-71765, 1975 (and Proc. Conf. on In-Situ Composites-II, Bolton Landing, N. Y., Xerox Individual Publ., 1976, pp. 27-36).

9. Johnston, James R.; and Ashbrook, Richard L.: Oxidation and Thermal Fatigue Cracking of Nickel- and Cobalt-Base Alloys in a High Velocity Gas Stream. NASA TN D-5376, 1969.

10. Sheffler, K. E.; et al.: Alloy and Structural Optimization of a Directionally Solidified Lamellar Eutectic Alloy. (PWA-5300, Pratt & Whitney Aircraft; NAS3-17811) NASA CR-135000, 1976.

11. ASTM Standard Recommended Practice E562-76 for Determining Volume Fraction by Systematic Manual Point Count. 1976 Annual Book of ASTM Standards, part 11.

12. Smartt, H. B.; and Courtney, T. H.: On the Rod to Blade Transition in the Al-$Al_3Ni$ Eutectic. Met. Trans., vol. 3, no. 7, July 1972, pp. 2000-2002.

13. Cooksey, D. J. S.; et al.: The Freezing of Some Continuous Binary Eutectic Mixtures. Phil. Mag., vol. 10, no. 107, Nov. 1964, pp. 745-769.

14. Rinaldi, M. D.; Sharp, R. M.; and Flemings, M. C.: Growth of Ternary Composites from the Melt: Part II. Met. Trans., vol. 3, no. 12, Dec. 1972, pp. 3139-3148.

15. Gray, H. R.; and Sanders, W. A.: Effect of Thermal Cycling in a Mach 0.3 Burner Rig on Properties and Structure of Directionally Solidified $\gamma/\gamma'$ - $\delta$ Eutectic. NASA TM X-3271 (and Proc. Conf. on In-Situ Composites-II, Bolton Landing, N. Y., Xerox Individual Publ., 1976, pp. 201-210).

16. Tewari, Surendra N.: Directionally Solidified Eutectic Alloy, $\gamma$ - $\beta$. NASA TN D-8355, 1976.

17. Dunlevey, F. M.; and Wallace, J. F.: The Effect of Thermal Cycling on the Structure and Properties of a Co, Cr, Ni - TaC Directionally Solidified Eutectic Alloy. Met. Trans., vol. 5, no. 6, June 1974, pp. 1351-1356.

18. Walter, J. L.; and Cline, H. E.: Stability of the Directionally Solidified Eutectics NiAl-Cr and NiAl-Mo. Met. Trans., vol. 4, no. 1, Jan. 1973, pp. 33-38.

19. Tittmann, B. R.; Nadler, H.; and Paton, N. E.: A Technique for Studies of Ductile Fracture in Metals Containing Voids or Inclusions. Met. Trans., vol. 7A, no. 2, Feb. 1976, pp. 320-323.

TABLE I. - RAW MATERIALS

| Element | Purity, wt % | Form |
|---|---|---|
| Ni | 99.9 | Elecholytic chips |
| Cr | 99.8 | Elecholytic chips |
| Fe | 99.8 | Chips |
| Ta | 99.5 | Chips |
| Nb | 99.5 | Chips |

TABLE II. - TEMPERATURE DEPENDENCE OF TENSILE PROPERTIES

OF IRON-BASE EUTECTIC ALLOYS

| Composition, wt % | Temperature, °C | Ultimate tensile strength | | Reduction of area, percent | Plastic elongation, percent | Yield strength | |
|---|---|---|---|---|---|---|---|
| | | MPa | ksi | | | MPa | ksi |
| Fe-15.5Nb-14.5Ni-6.0Cr | 1100 | 174 | 25.3 | 9 | 6.4 | 172 | 24.9 |
| | 750 | 425 | 61.7 | 2 | 0 | 425 | 61.7 |
| | 25 | 785 | 113.9 | 2 | 0 | 785 | 113.9 |
| Fe-25Ta-22Ni-10Cr | 1100 | 187 | 28.1 | 8 | 12 | 183 | 26.5 |
| | 1100 | 162 | 23.5 | 3 | 8 | 145 | 21.0 |
| | 750 | 588 | 85.4 | 3 | 2 | 588 | 85.4 |
| | 750 | 547 | 79.5 | 0 | 0 | 547 | 79.5 |
| | 25 | 922 | 133.9 | 0 | 0 | 907 | 131.5 |

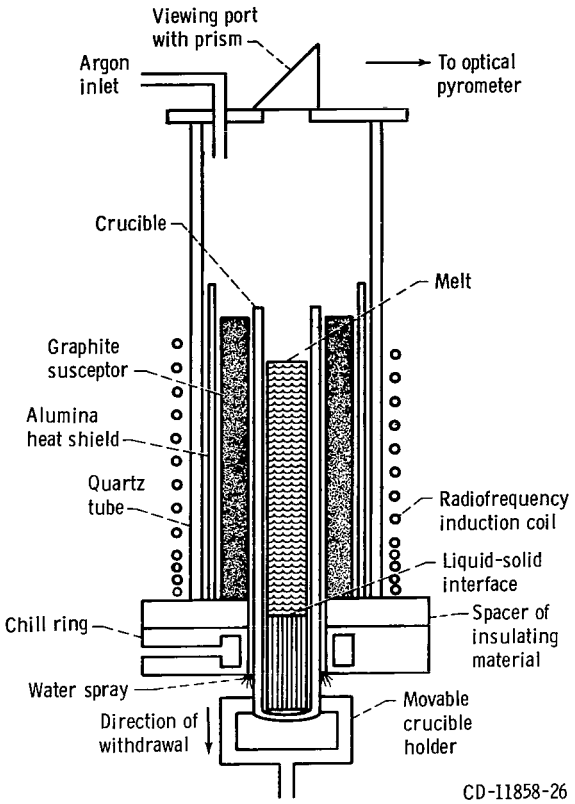


Figure 1. - Bridgman directional solidification apparatus.

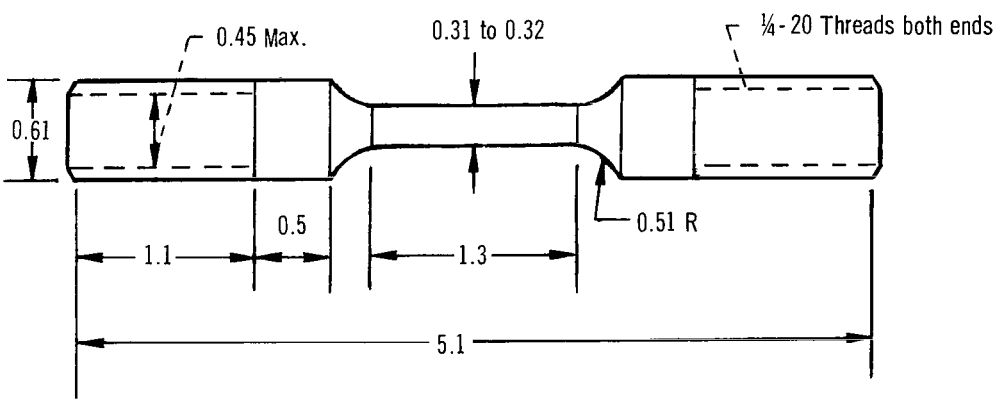


Figure 2. - Tensile test specimen. (Dimensions are in cm, except thread specification, which is in inches.)

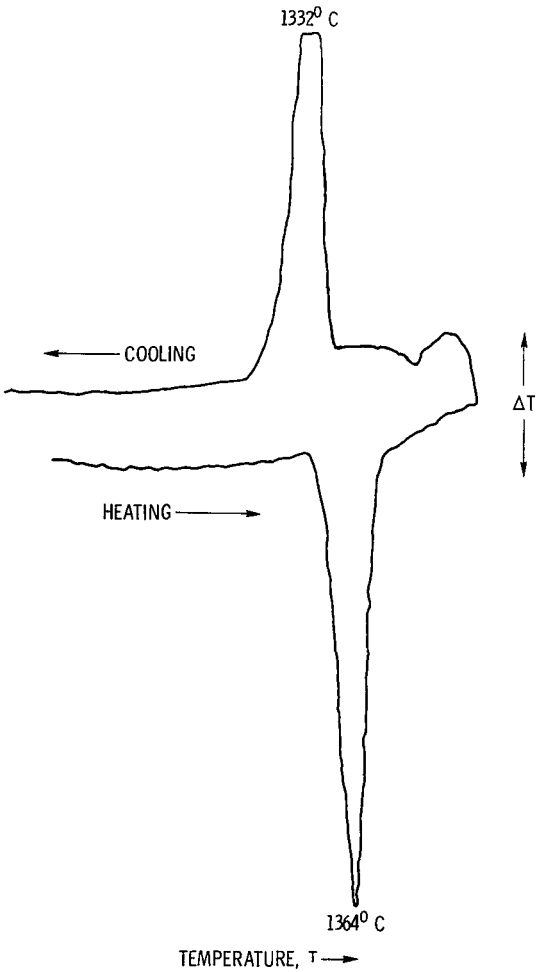


(a) Differential thermal analysis of Fe-25Ta-22Ni-10Cr.

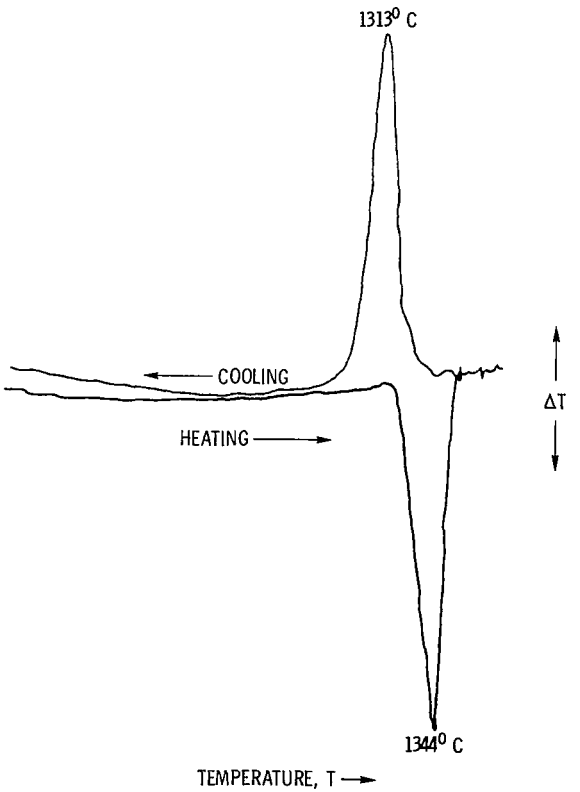


(b) Differential thermal analysis of Fe-15.5Nb-14.5Ni-6.0Cr.

Figure 3. - Differential thermal analysis trace of iron-base eutectic alloys.

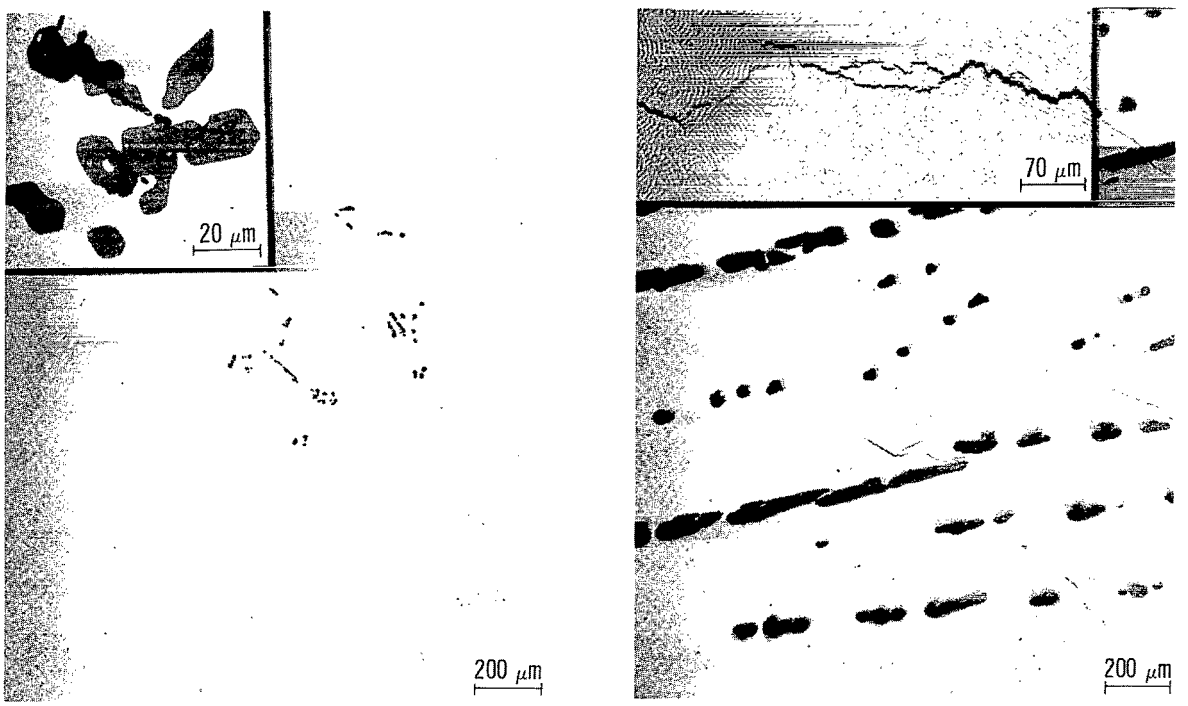


(a) 2.6 Centimeters from bottom.

(b) 8.5 Centimeters from bottom.

Figure 4. - Appearance and distribution of inclusions in directionally solidified, $\gamma$ - $\epsilon$ eutectic alloy Fe-15.5Nb-14.5Ni-6.0Cr. Transverse light micrographs; melt temperature, 1760° C.

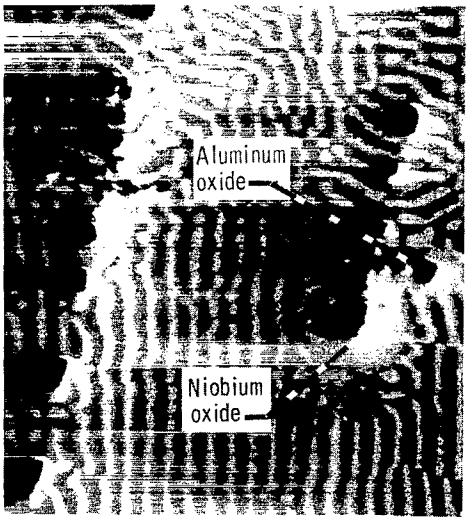


(a) Secondary electron micrograph.

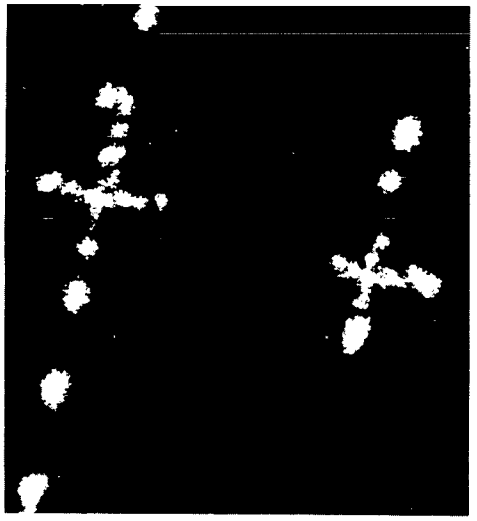

(b) Aluminum $K_\alpha$ X-ray raster micrograph.

(c) Niobium $L_\alpha$ X-ray raster micrograph.

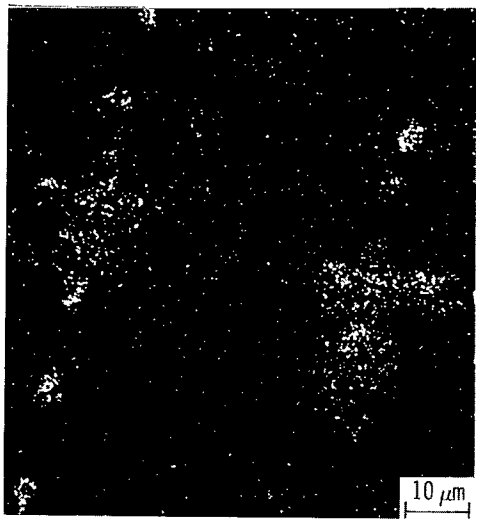


(d) Oxygen $K_\alpha$ X-ray raster micrograph.

Figure 5. - Identification of aluminum oxide and niobium oxide inclusions in directionally solidified eutectic alloy Fe-15.5Nb-14.5Ni-6.0Cr.

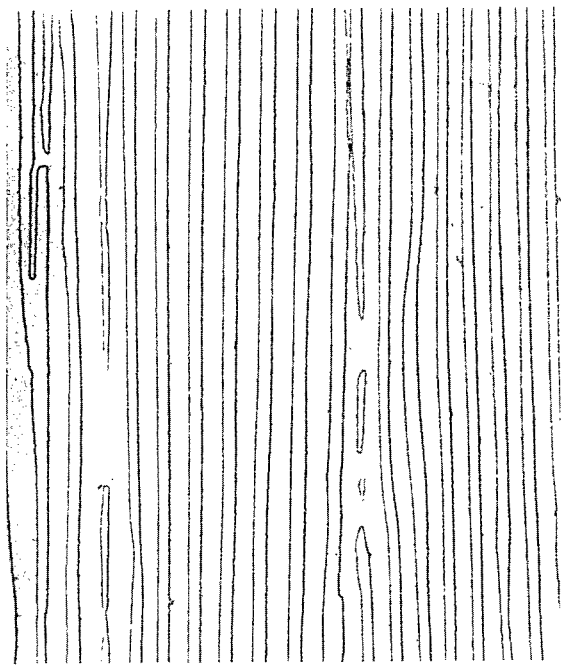

(a) Longitudinal.


(b) Transverse.

Figure 6. - Microstructure of directionally solidified eutectic alloy Fe-15.5Nb-14.5Ni-6.0Cr.

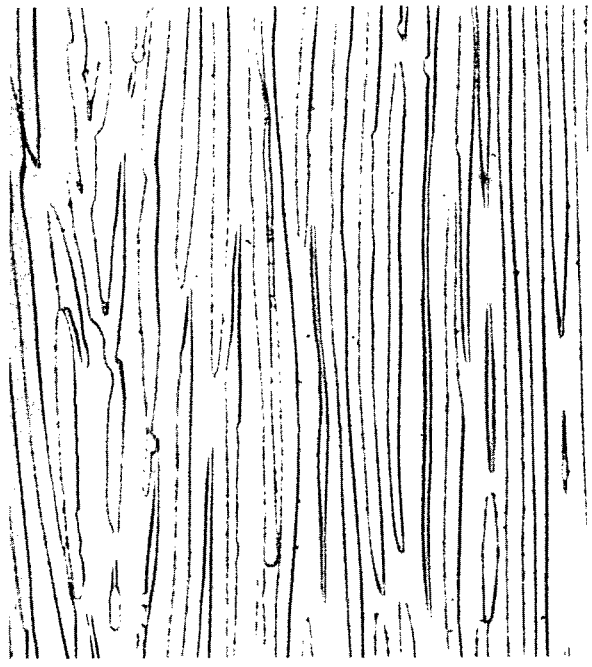

(a) Longitudinal.

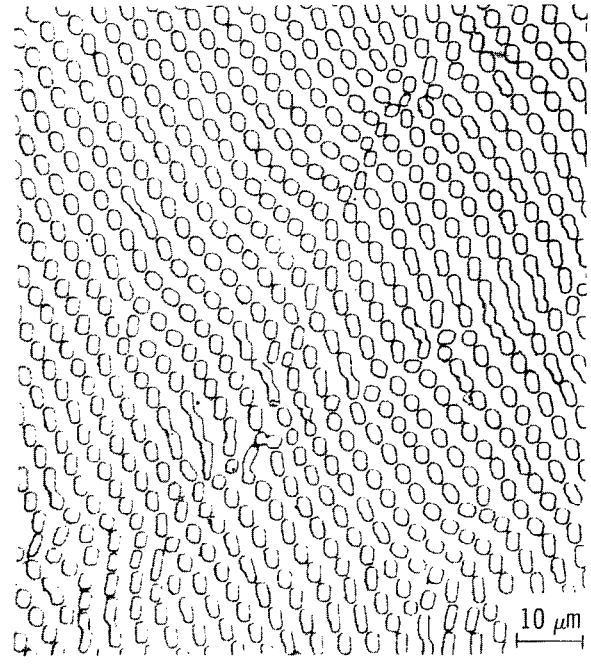


(b) Transverse.

Figure 7. - Microstructure of directionally solidified eutectic alloy Fe-25Ta-22Ni-10Cr.

(a) Directionally solidified.

(b) Thermally cycled.


(c) Thermally cycled, at oxidized surface.

Figure 8. - Effect of 1800 thermal cycles (1100° to 425° C at 3-min intervals) on microstructure of directionally solidified eutectic alloy Fe-25Ta-22Ni-10Cr.

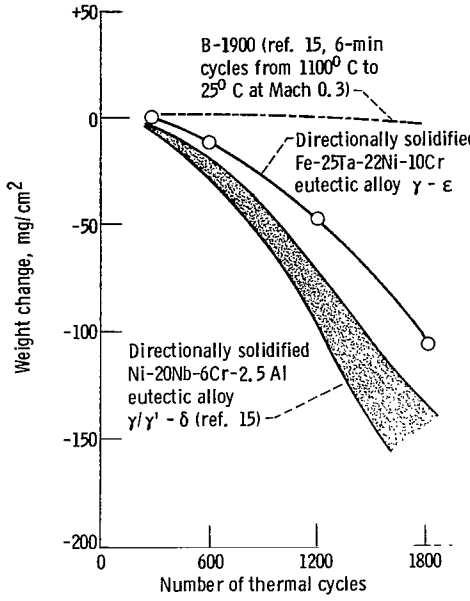


Figure 9. - Specific weight change in directionally solidified eutectic alloy Fe-25Ta-22Ni-10Cr due to thermal cycling.

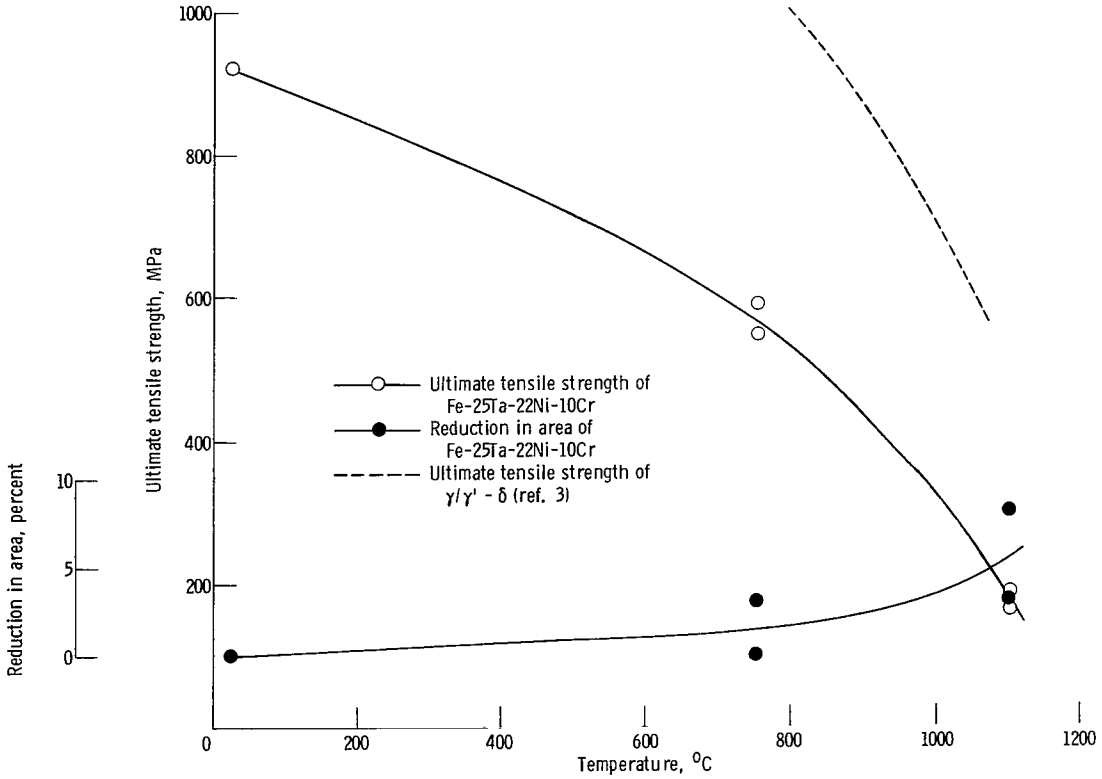


Figure 10. - Effect of temperature on tensile properties of directionally solidified eutectic alloy Fe-25Ta-22Ni-10Cr.

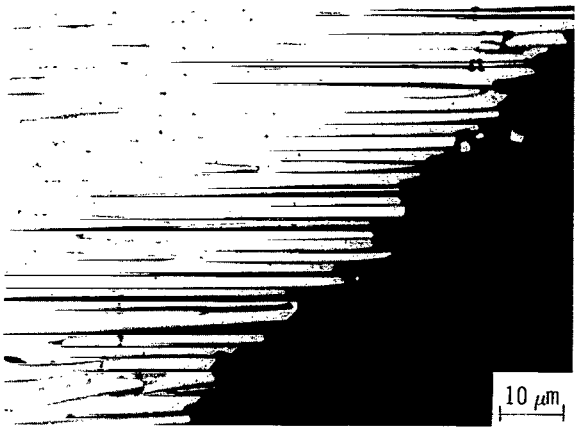


(a) Room temperature.

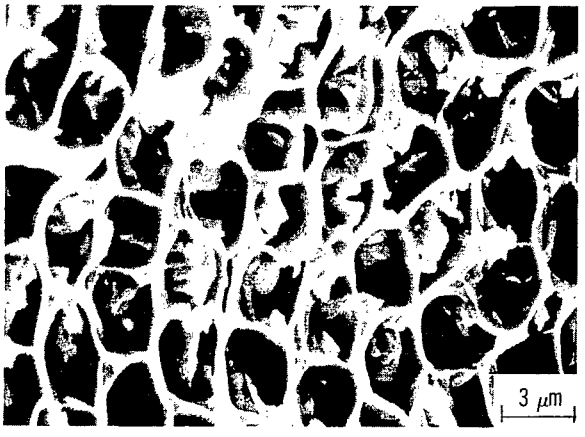


(b) Room temperature (SEM micrograph).

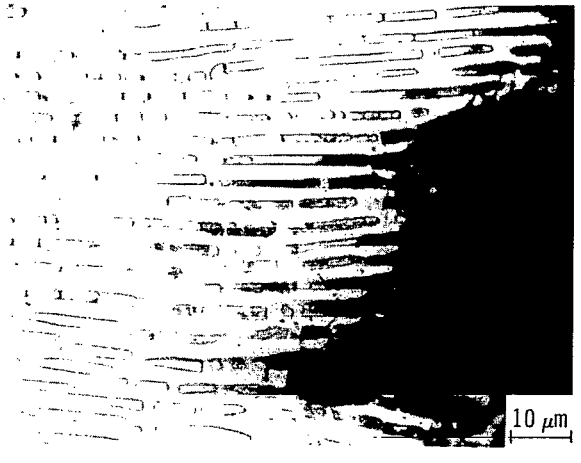


(c) Temperature, 1100° C.

Figure 11. - Effect of temperature on tensile fracture morphology of directionally solidified eutectic alloy Fe-25Ta-22Ni-10Cr.

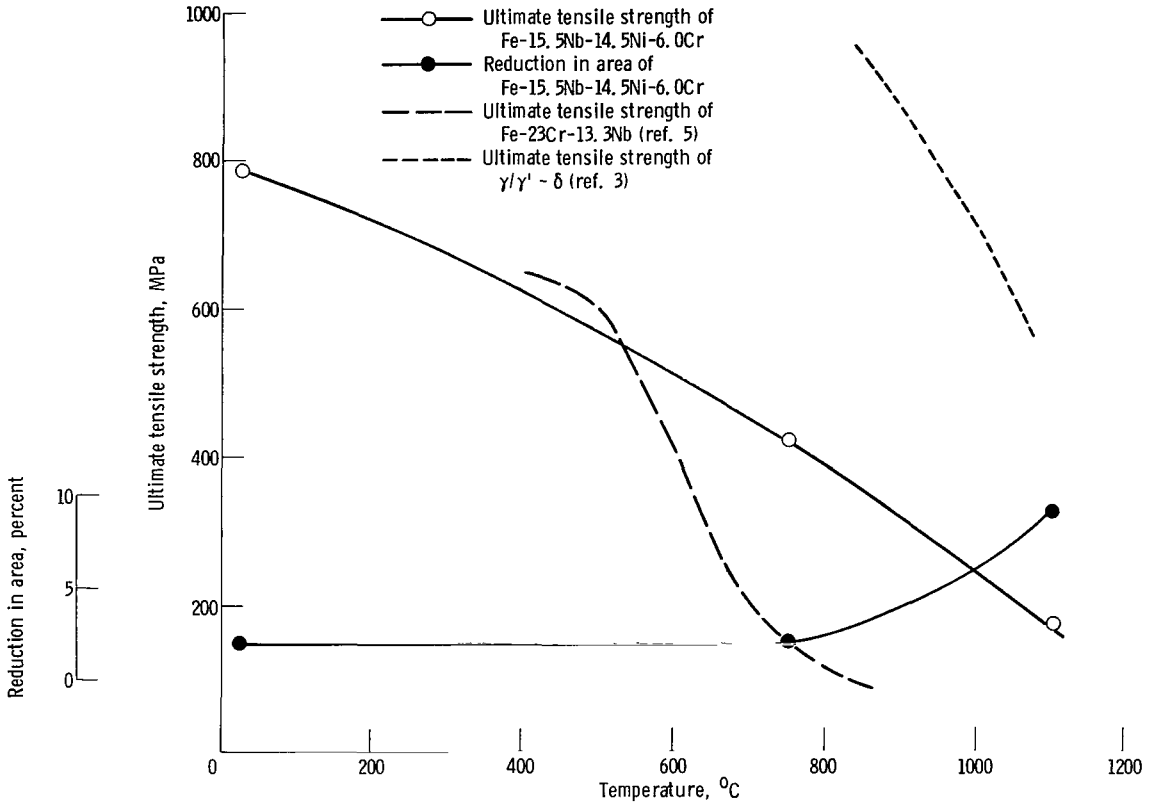


Figure 12. - Effect of temperature on tensile properties of directionally solidified eutectic alloy Fe-15.5Nb-14.5Ni-6.0Cr.

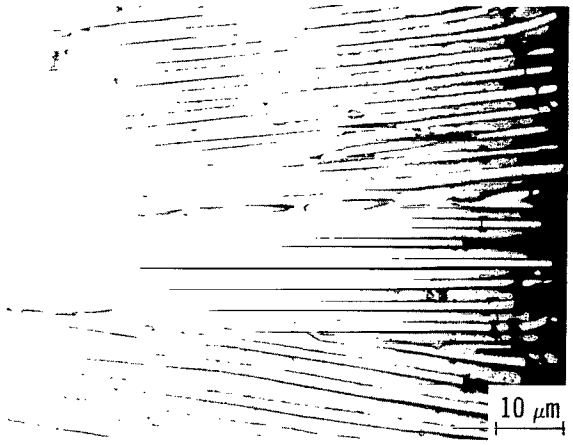


(a) Room temperature.


(b) Room temperature (SEM micrograph).


(c) Temperature, 1100° C.

Figure 13. - Effect of temperature on tensile fracture morphology of directionally solidified eutectic alloy Fe-15.5Nb-14.5Ni-6.0Cr.

*"The aeronautical and space activities of the United States shall be conducted so as to contribute . . . to the expansion of human knowledge of phenomena in the atmosphere and space. The Administration shall provide for the widest practicable and appropriate dissemination of information concerning its activities and the results thereof."*

—NATIONAL AERONAUTICS AND SPACE ACT OF 1958

# NASA SCIENTIFIC AND TECHNICAL PUBLICATIONS

TECHNICAL REPORTS: Scientific and technical information considered important, complete, and a lasting contribution to existing knowledge.

TECHNICAL NOTES: Information less broad in scope but nevertheless of importance as a contribution to existing knowledge.

TECHNICAL MEMORANDUMS: Information receiving limited distribution because of preliminary data, security classification, or other reasons. Also includes conference proceedings with either limited or unlimited distribution.

CONTRACTOR REPORTS: Scientific and technical information generated under a NASA contract or grant and considered an important contribution to existing knowledge.

TECHNICAL TRANSLATIONS: Information published in a foreign language considered to merit NASA distribution in English.

SPECIAL PUBLICATIONS: Information derived from or of value to NASA activities. Publications include final reports of major projects, monographs, data compilations, handbooks, sourcebooks, and special bibliographies.

TECHNOLOGY UTILIZATION PUBLICATIONS: Information on technology used by NASA that may be of particular interest in commercial and other non-aerospace applications. Publications include Tech Briefs, Technology Utilization Reports and Technology Surveys.

***Details on the availability of these publications may be obtained from:***

**SCIENTIFIC AND TECHNICAL INFORMATION OFFICE**

**NATIONAL AERONAUTICS AND SPACE ADMINISTRATION**

**Washington, D.C. 20546**